Convex Programming with Separable Ellipsoidal Constraints: Application in Contact Problems with Orthotropic Friction

Jaroslav Haslinger, Radek Kučera, and Tomáš Kozubek

Abstract This contribution presents an algorithm for constrained minimization of strictly convex quadratic functions subject to simple bounds and separable ellipsoidal constraints. The algorithm is used for numerical solution of discretized 3D contact problems with orthotropic friction. These problems have been solved by a polygonal approximation of the friction cone. Our algorithm enables us to use the original friction cone without any approximation. Results of model examples are shown.

Keywords Contact problems with orthotropic friction • Convex programming • Separable ellipsoidal constraints

Mathematics Subject Classification (2010). Primary 90C25; Secondary 35J86, 49M25, 74P10.

1 Introduction

Methods for numerical minimization of quadratic functions subject to convex constraints have been intensively developed in last decades [1–3,17] and nowadays they are an inherent part of many packages. These methods, however, are integrated into the packages in a fairly general setting. Therefore, they usually cannot be directly used in large scale problems arising, e.g., from finite element approximations. For this reason, the development of methods which take into account specifics of problems to be solved is important. Potential features which may be beneficial are

J. Haslinger (✉)
KNM MFF UK, Sokolovská 83, 18675 Praha 8, Czech Republic
e-mail: hasling@karlin.mff.cuni.cz

R. Kučera • T. Kozubek
IT4Innovations, VŠB-TUO, 17. listopadu 15, 70833 Ostrava, Czech Republic
e-mail: radek.kucera@vsb.cz; tomas.kozubek@vsb.cz

R. Hoppe (ed.), *Optimization with PDE Constraints*, Lecture Notes in Computational Science and Engineering 101,
DOI 10.1007/978-3-319-08025-3_7

the following: *a)* the number of variables subject to constraints is much lower than the total number of all variables; *b)* each variable appears in one constraint at most, i.e., the constraints are separable. In [13, 14], the author introduced and analyzed a new method for minimization of strictly convex quadratic functions with separable convex constraints. The separable character of constraints simplified the analysis that was based on the Karusch-Kuhn-Tucker (KKT) conditions. Their geometrical interpretation enabled to generalize an idea of the reduced gradient introduced originally for simple bound problems [4]. The resulting algorithm is closely related to the Rosen method [16]. Clearly, the efficient implementation of the algorithm strongly depends on the specific form of the constraint functions.

This study was motivated by necessity to solve numerically 3D contact problems with friction [10]. So far such problems have been solved by a polygonal approximation of the Coulomb friction cone [18]. The presented algorithm enables us to use the original Coulomb friction cone without any approximation. Since the number of unilateral constraints describing contact conditions is much smaller in comparison with the total number of all variables (hence *a)*), one of the efficient approaches for solving such problems is based on an appropriate discretization of the dual variational formulation, i.e., the formulation in terms of the Lagrange multipliers which are defined on the contact boundary. There are two vectors of the Lagrange multipliers in the discrete setting of frictional contact problems: one, denoted as $\bar{\boldsymbol{\lambda}}_\nu$, releases the unilateral constraints and is subject only to a sign condition; the second one, denoted as $\bar{\boldsymbol{\lambda}}_t := (\bar{\boldsymbol{\lambda}}_{t_1}, \bar{\boldsymbol{\lambda}}_{t_2})$, regularizes the non-smooth frictional term and is subject to convex constraints imposed on disjoint pairs of its components (hence *b)*). For an isotropic friction law, when frictional effects are the same in all directions, the constraints reduce to simple circular (spherical) ones, i.e., the zero level sets of the constraint functions are circles in $\mathbb{R}^2$.

The aim of the contribution is to extend this method to the case of separable ellipsoidal constraints. A simple change of variables permits to transform the ellipsoidal constraints to the circular ones. In computations, however, it turns out that the original setting (i.e., with the ellipsoidal constraints) is usually better for the performance of the algorithm, especially, in the case of strongly eccentric ellipses. Again, the minimization of functions with this type of constraints was motivated by practical needs. Indeed, the dual variational formulation of 3D contact problems with orthotropic friction (i.e., friction effects are now different in two à-priori given perpendicular directions) leads to separable ellipsoidal constraints for pairs made of the components of $\bar{\boldsymbol{\lambda}}_t$.

The paper is organized as follows. In Sect. 2 we shortly recall results from [13, 14]. The main attention will be paid to the numerical computation of the projection onto the ellipse which is an important ingredient of our algorithm. Unlike the projection onto the circle, this one is far from to be so simple. Finally in Sect. 3, we first derive the algebraic form of the dual formulation of 3D contact problems with orthotropic Coulomb friction and then, in Sect. 4, we apply our algorithms to several model examples.

2 Minimization Subject to Separable Ellipsoidal Constraints

In this section, we consider the following problem:

$$\text{find} \quad \bar{\mathbf{x}}^* = \arg\min\{q(\bar{\mathbf{x}}) : \bar{\mathbf{x}} \in \Lambda\}, \tag{2.1}$$

where $q(\bar{\mathbf{x}}) = \frac{1}{2}\bar{\mathbf{x}}^\top \mathbf{A}\bar{\mathbf{x}} - \bar{\mathbf{x}}^\top \bar{\mathbf{b}}$ with symmetric, positive definite $\mathbf{A} \in \mathbb{R}^{n\times n}$, $\bar{\mathbf{b}}, \bar{\mathbf{x}} \in \mathbb{R}^n$, $\bar{\mathbf{x}} = (x_1, \ldots, x_n)^\top$, $n = 3m$, and $\Lambda = \Lambda_1 \times \cdots \times \Lambda_{2m}$ defined by

$$\Lambda_i = \{x_i \in \mathbb{R} : x_i \geq l_i\},$$

$$\Lambda_{i+m} = \{(x_{i+m}, x_{i+2m})^\top \in \mathbb{R}^2 : \left(\frac{x_{i+m} - c_i}{a_i}\right)^2 + \left(\frac{x_{i+2m} - c_{i+m}}{a_{i+m}}\right)^2 \leq g_i^2\}$$

with given $l_i, c_i, c_{i+m} \in \mathbb{R}$, $g_i, a_i, a_{i+m} \in \mathbb{R}_+$ for $i = 1, \ldots, m$. As q is strictly convex on the closed covex set Λ, there is a unique solution $\bar{\mathbf{x}}^* \in \Lambda$ to (2.1). Before we give ideas of the active-set KPRGP algorithm (KKT Proportioning with Reduced Gradient Projections) analyzed in [7, 14], we introduce notation.

Let $\mathcal{N} = \{1, \ldots, n\}$ be the set of all indices and let $\mathcal{A}(\bar{\mathbf{x}}) \subseteq \mathcal{N}$ be the subset of indices of active constraints at $\bar{\mathbf{x}} \in \Lambda$:

$$\mathcal{A}(\bar{\mathbf{x}}) = \{i : x_i = l_i,\ 1 \leq i \leq m\}$$

$$\bigcup\{j : j = i + m, \left(\frac{x_{i+m} - c_i}{a_i}\right)^2 + \left(\frac{x_{i+2m} - c_{i+m}}{a_{i+m}}\right)^2 = g_i^2,\ 1 \leq i \leq m\}$$

$$\bigcup\{j : j = i + 2m, \left(\frac{x_{i+m} - c_i}{a_i}\right)^2 + \left(\frac{x_{i+2m} - c_{i+m}}{a_{i+m}}\right)^2 = g_i^2, 1 \leq i \leq m\}.$$

Let $\bar{\mathbf{r}}(\bar{\mathbf{x}}) = \mathbf{A}\bar{\mathbf{x}} - \bar{\mathbf{b}}$ denote the gradient of q at $\bar{\mathbf{x}} \in \mathbb{R}^n$. The orthogonal projection $\mathbf{P}_\Lambda$ onto Λ at $\bar{\mathbf{x}} \in \mathbb{R}^n$ is defined by

$$\mathbf{P}_\Lambda(\bar{\mathbf{x}}) = \arg\min_{\bar{\mathbf{y}}\in\Lambda} \|\bar{\mathbf{y}} - \bar{\mathbf{x}}\|. \tag{2.2}$$

As Λ is separable, $\mathbf{P}_\Lambda$ may be split into single projections P_{Λ_i} onto Λ_i. Let us introduce the *reduced gradient* of q at $\bar{\mathbf{x}} \in \Lambda$ for a fixed $\alpha > 0$ by:

$$\bar{\mathbf{r}}^{red}(\bar{\mathbf{x}}) = \frac{1}{\alpha}(\bar{\mathbf{x}} - \mathbf{P}_\Lambda(\bar{\mathbf{x}} - \alpha\bar{\mathbf{r}}(\bar{\mathbf{x}}))).$$

Note that the reduced gradient characterizes the optimality criterion to (2.1). Indeed, $\bar{\mathbf{x}}^*$ is the solution to (2.1) iff $\bar{\mathbf{r}}^{red}(\bar{\mathbf{x}}^*) = \mathbf{0}$. Moreover, if $\bar{\mathbf{x}} \neq \bar{\mathbf{x}}^*$ and $\alpha > 0$

is sufficiently small, then the negative reduced gradient $-\bar{\mathbf{r}}^{red}(\bar{\mathbf{x}})$ is a decrease direction at $\bar{\mathbf{x}} \in \Lambda$. To change appropriately the active set, we decompose $\bar{\mathbf{r}}^{red} := \bar{\mathbf{r}}^{red}(\bar{\mathbf{x}})$ into the *free reduced gradient* $\bar{\boldsymbol{\varphi}} := \bar{\boldsymbol{\varphi}}(\bar{\mathbf{x}})$ and the *chopped reduced gradient* $\bar{\boldsymbol{\psi}} := \bar{\boldsymbol{\psi}}(\bar{\mathbf{x}})$ as follows:

$$\bar{\boldsymbol{\varphi}}_{\mathcal{A}} = \mathbf{0}, \quad \bar{\boldsymbol{\varphi}}_{\mathcal{N}\setminus\mathcal{A}} = \bar{\mathbf{r}}^{red}_{\mathcal{N}\setminus\mathcal{A}},$$
$$\bar{\boldsymbol{\psi}}_{\mathcal{A}} = \bar{\mathbf{r}}^{red}_{\mathcal{A}}, \ \bar{\boldsymbol{\psi}}_{\mathcal{M}\setminus\mathcal{A}} = \mathbf{0},$$

where $\bar{\boldsymbol{\varphi}}_{\mathcal{A}}$ and $\bar{\boldsymbol{\varphi}}_{\mathcal{N}\setminus\mathcal{A}}$ denote the sub-vectors of $\bar{\boldsymbol{\varphi}}$ with components determined by the indices of $\mathcal{A} := \mathcal{A}(\bar{\mathbf{x}})$ and $\mathcal{N} \setminus \mathcal{A}$, respectively (similarly for $\bar{\mathbf{r}}^{red}$ and $\bar{\boldsymbol{\psi}}$).

We combine the following three steps to generate a sequence $\{\bar{\mathbf{x}}^{(l)}\}$ that approximates the solution $\bar{\mathbf{x}}^*$:

- the *expansion step*: $\bar{\mathbf{x}}^{(l+1)} = \bar{\mathbf{x}}^{(l)} - \alpha\bar{\boldsymbol{\varphi}}(\bar{\mathbf{x}}^{(l)})$,
- the *proportioning step*: $\bar{\mathbf{x}}^{(l+1)} = \bar{\mathbf{x}}^{(l)} - \alpha\bar{\boldsymbol{\psi}}(\bar{\mathbf{x}}^{(l)})$,
- the *conjugate gradient step*: $\bar{\mathbf{x}}^{(l+1)} = \bar{\mathbf{x}}^{(l)} - \alpha^{(l)}_{cg}\bar{\mathbf{p}}^{(l)}$, where the step-length $\alpha^{(l)}_{cg}$ and the conjugate gradient directions $\bar{\mathbf{p}}^{(l)}$ are computed recurrently [8]; the recurrence starts from $\bar{\mathbf{x}}^{(s)}$ generated by the last expansion or the proportioning step and satisfies $\mathcal{A}(\bar{\mathbf{x}}^{(l+1)}) = \mathcal{A}(\bar{\mathbf{x}}^{(s)})$.

The expansion step may add while the proportioning step may remove indices to/from the current active set. The conjugate gradient steps are used to carry out efficiently the minimization of q in the interior of the face $W(\bar{\mathbf{x}}^{(s)}) = \{\bar{\mathbf{x}} \in \Lambda \,|\, \bar{\mathbf{x}}_{\mathcal{A}} = \bar{\mathbf{x}}^{(s)}_{\mathcal{A}}, \mathcal{A} := \mathcal{A}(\bar{\mathbf{x}}^{(s)})\}$. Moreover, the algorithm exploits a given constant $\Gamma > 0$ in the *proportioning criterion*

$$\bar{\boldsymbol{\psi}}(\bar{\mathbf{x}}^{(l)})^\top \bar{\mathbf{r}}(\bar{\mathbf{x}}^{(l)}) \le \Gamma\ \bar{\boldsymbol{\varphi}}(\bar{\mathbf{x}}^{(l)})^\top \bar{\mathbf{r}}(\bar{\mathbf{x}}^{(l)}) \tag{2.3}$$

to decide which of the steps will be performed.

Algorithm KPRGP

Let $\bar{\mathbf{x}}^{(0)} \in \Lambda$, $\Gamma > 0$, $\alpha \in (0, 2\|\mathbf{A}\|^{-1})$, and $\varepsilon > 0$ be given. For $\bar{\mathbf{x}}^{(l)}$, $\bar{\mathbf{x}}^{(s)}$ known, $0 \le s \le l$, where $\bar{\mathbf{x}}^{(s)}$ is computed by the last expansion or proportioning step, choose $\bar{\mathbf{x}}^{(l+1)}$ by the following rules:

(i). If $\|\bar{\mathbf{r}}^{red}(\bar{\mathbf{x}}^{(l)})\| \le \varepsilon$, return $\bar{\mathbf{x}} = \bar{\mathbf{x}}^{(l)}$.

(ii). If $\bar{\mathbf{x}}^{(l)}$ fulfils (2.3), try to generate $\bar{\mathbf{x}}^{(l+1)}$ by the conjugate gradient step. If $\bar{\mathbf{x}}^{(l+1)} \in \operatorname{Int} W(\bar{\mathbf{x}}^{(s)})$, accept it, otherwise generate $\bar{\mathbf{x}}^{(l+1)}$ by the expansion step.

(iii). If $\bar{\mathbf{x}}^{(l)}$ does not fulfil (2.3), generate $\bar{\mathbf{x}}^{(l+1)}$ by the proportioning step.

The convergence rate of this algorithm derived in [14] does not depend on the type of convex constraints. However, the implementation requires to compute the projection $\mathbf{P}_\Lambda$ via the single projections P_{Λ_i} and $P_{\Lambda_{i+m}}$, $1 \le i \le m$. In the rest of this section we show how to compute these projections.

The set Λ_i, $i = 1, \ldots, m$ represents the simple bound for which the projection is trivial:

$$P_{\Lambda_i}(x_i) = \begin{cases} x_i & \text{if } x_i \geq l_i, \\ l_i & \text{otherwise.} \end{cases}$$

The projection onto Λ_{i+m}, $i = 1, \ldots, m$ is more involved. To simplify our presentation we denote $\mathbf{x}_i = (x_{i+m}, x_{i+2m})^\top \in \mathbb{R}^2$ and $\mathbf{c}_i = (c_i, c_{i+m})^\top \in \mathbb{R}^2$. The corresponding projection is given by

$$P_{\Lambda_{i+m}}(\mathbf{x}_i) = \begin{cases} \mathbf{x}_i & \text{if } \left(\dfrac{x_{i+m} - c_i}{a_i}\right)^2 + \left(\dfrac{x_{i+2m} - c_{i+m}}{a_{i+m}}\right)^2 \leq g_i^2, \\ \mathbf{y}_i & \text{otherwise,} \end{cases}$$

where we will specify how to get $\mathbf{y}_i \in \mathbb{R}^2$. We distinguish two situations. If $a_i = a_{i+1}$, then Λ_{i+m} describes the circular constraint for which $\mathbf{y}_i$ is given by the explicit formula:

$$\mathbf{y}_i = \mathbf{c}_i + \frac{a_i g_i}{\|\mathbf{x}_i - \mathbf{c}_i\|}(\mathbf{x}_i - \mathbf{c}_i). \tag{2.4}$$

If $a_i \neq a_{i+1}$, then $\mathbf{y}_i$ is the closest point to $\mathbf{x}_i$ lying on the ellipse $\mathbf{e}_i := \mathbf{e}_i(t)$ (in the parametric representation):

$$\mathbf{e}_i(t) = \mathbf{c}_i + g_i \begin{pmatrix} a_i \cos t \\ a_{i+m} \sin t \end{pmatrix}, \quad t \in [0, 2\pi).$$

Let t^* be the value of t such that $\mathbf{y}_i = \mathbf{e}_i(t^*)$. Such t^* satisfies the following orthogonality condition:

$$(\mathbf{x}_i - \mathbf{e}_i(t))^\top \mathbf{e}_i'(t) = 0. \tag{2.5}$$

Although (2.5) is the equation in $\mathbb{R}^1$, its solution is not unique. The reason is that (2.5) is equivalent to the fourth degree polynomial equation with either two or four roots. Fortunately, one can recognize correct t^* characterized by the fact that $\mathbf{y}_i$ belongs to the same quadrant as $\mathbf{x}_i$, provided that the local coordinate system (in $\mathbb{R}^2$) coincides with the half-axes of the ellipse. To perform efficiently computations of t^* via (2.5), we combine the Newton and bisection methods (in $\mathbb{R}^1$). The resulting algorithm may benefit from fast convergence of the Newton iterations while the bisection steps ensure convergence to t^*. A long sequence of bisection steps are generated in situations when the root t^* is close to an inflection point of the function in (2.5) (that is not excluded in general).

Remark 2.1. Another way how to solve (2.1) by ALGORITHM KPRGP consists in transforming the ellipsoidal constraints to the circular ones using the substitution:

$$\bar{\mathbf{y}} = \mathbf{D}^{-1}\bar{\mathbf{x}},$$

where $\mathbf{D} = diag(1, \dots, 1, a_1, \dots, a_{2m}) \in \mathbb{R}^{n\times n}$. This leads to the problem in terms of the new variable $\bar{\mathbf{y}}$:

$$\text{find} \quad \bar{\mathbf{y}}^* = \arg\min\{q(\bar{\mathbf{y}}) : \ \bar{\mathbf{y}} \in \Lambda\}, \tag{2.6}$$

where $q(\bar{\mathbf{y}}) = \frac{1}{2}\,\bar{\mathbf{y}}^\top \mathbf{DAD}\bar{\mathbf{y}} - \bar{\mathbf{y}}^\top \mathbf{D}\bar{\mathbf{b}}$ and $\Lambda = \Lambda_1 \times \cdots \times \Lambda_{2m}$ is defined by

$$\Lambda_i = \{y_i \in \mathbb{R} : \ y_i \geq l_i\},$$

$$\Lambda_{i+m} = \{(y_{i+m}, y_{i+2m})^\top \in \mathbb{R}^2 : \ (y_{i+m} - d_i)^2 + (y_{i+2m} - d_{i+m})^2 \leq g_i^2\},$$

with $d_i = c_i/a_i$, $d_{i+m} = c_{i+m}/a_{i+m}$ for $i = 1, \dots, m$. Problem (2.6) is the special case of (2.1) for which the projections can be computed by (2.4). On the other hand, the condition number of **DAD** is usually greater than the one of **A**, especially, when the ellipses in the original problem are strongly eccentric. In this case, the convergence factor of ALGORITHM KPRGP derived in [14] is smaller for (2.1) that may result in a better performance of computations.

3 Numerical Solution of 3D Contact Problems with Orthotropic Coulomb Friction

The minimization algorithm from the previous section will be now used for the numerical solution of 3D contact problems with orthotropic Coulomb friction. Recall that contact mechanics is a branch of mechanics of solids which studies the behavior of loaded systems of deformable bodies being in mutual contact. Mathematical models of such problems are given by equations involving non-smooth multivalued mappings due to non-penetration and friction conditions on common parts of the boundary. In contrast to isotropic friction, effects of orthotropic friction are different in directions of two orthogonal orthotropy axis. We first present the weak formulation of such problems, then we give their finite element discretization and the transformation of the resulting algebraic problem into a new one having a structure required by the algorithm KPRGP.

Our system consists of two elastic bodies represented by *polyhedral* domains $\Omega^k \subset \mathbb{R}^3$ whose boundaries are split into three disjoint parts Γ_u^k, Γ_p^k, and Γ_c^k, $k = 1, 2$. Denote $\Omega = \Omega^1 \cup \Omega^2$, $\Gamma_u = \Gamma_u^1 \cup \Gamma_u^2$, $\Gamma_p = \Gamma_p^1 \cup \Gamma_p^2$, and $\Gamma_c = \Gamma_c^1 \cup \Gamma_c^2$. The zero displacements will be prescribed on Γ_u, while surface tractions of density $\mathbf{p} \in (L^2(\Gamma_p))^3$ act on Γ_p. Both bodies are in contact along Γ_c^1 and Γ_c^2 in

the undeformed state. In what follows we shall suppose that $\Gamma_u^k \neq \emptyset, k = 1, 2$ and $\Gamma_c^1 = \Gamma_c^2$, i.e. there is no gap between Ω^1 and Ω^2. On Γ_c unilateral and friction conditions will be prescribed. Finally, Ω is subject to body forces of density $\mathbf{f} \in (L^2(\Omega))^3$. Our aim is to find an equilibrium state of this system.

Before we give the weak formulation of this problem, we introduce several notation and function sets which will be needed. Let $\mathbf{u} : \Omega \mapsto \mathbb{R}^3$ be a deformation field in Ω and $\mathbf{u}^k := \mathbf{u}_{|\Omega^k}$ its restriction to $\Omega^k, k = 1, 2$. By $\boldsymbol{\epsilon}(\mathbf{u}) = \frac{1}{2}(\nabla\mathbf{u} + (\nabla\mathbf{u})^\top)$ we denote the linearized strain tensor, while $\boldsymbol{\sigma}(\mathbf{u})$ is the stress tensor linked to $\boldsymbol{\epsilon}(\mathbf{u})$ by means of a linear Hooke's law whose coefficients satisfy the usual symmetry and ellipticity conditions [15]. The outward unit normal vector to $\partial\Omega^1$ at a point $\mathbf{x} \in \Gamma_c$ is denoted as $\boldsymbol{\nu}(\mathbf{x})$. The orthotropy axis of friction at $\mathbf{x} \in \Gamma_c$ are given by a pair of orthogonal vectors $\mathbf{t}_1(\mathbf{x})$ and $\mathbf{t}_2(\mathbf{x})$ lying in the tangent plane to Γ_c at $\mathbf{x}$. The relative normal contact displacement at $\mathbf{x} \in \Gamma_c$ is defined by $u_\nu(\mathbf{x}) := (\mathbf{u}^1(\mathbf{x}) - \mathbf{u}^2(\mathbf{x}))^\top \boldsymbol{\nu}(\mathbf{x})$ and $\sigma_\nu(\mathbf{u}(\mathbf{x})) := \boldsymbol{\nu}^\top(\mathbf{x})\boldsymbol{\sigma}(\mathbf{u}^1(\mathbf{x}))\boldsymbol{\nu}(\mathbf{x})$ is the normal contact stress. Similarly, $\mathbf{u}_t(\mathbf{x}) = (u_{t_1}(\mathbf{x}), u_{t_2}(\mathbf{x}))^\top$, $\boldsymbol{\sigma}_t(\mathbf{u}(\mathbf{x})) = (\sigma_{t_1}(\mathbf{u}(\mathbf{x})), \sigma_{t_2}(\mathbf{u}(\mathbf{x})))^\top$ are the relative tangential contact displacement and the tangential contact stress at $\mathbf{x} \in \Gamma_c$, respectively, whose components are $u_{t_i}(\mathbf{x}) := (\mathbf{u}^1(\mathbf{x}) - \mathbf{u}^2(\mathbf{x}))^\top \mathbf{t}_i(\mathbf{x})$ and $\sigma_{t_i}(\mathbf{u}(\mathbf{x})) := \mathbf{t}_i{}^\top(\mathbf{x})\boldsymbol{\sigma}(\mathbf{u}^1(\mathbf{x}))\boldsymbol{\nu}(\mathbf{x}), i = 1, 2$. In addition to orthotropy axis, friction will be characterized by two positive, bounded and continuous functions $\mathcal{F}_1$ and $\mathcal{F}_2$ whose values at $\mathbf{x} \in \Gamma_c$ define coefficients of friction in directions $\mathbf{t}_1(\mathbf{x})$ and $\mathbf{t}_2(\mathbf{x})$, respectively. The diagonal (2×2) matrix $diag\{\mathcal{F}_1, \mathcal{F}_2\}$ will be denoted by $\boldsymbol{\mathcal{F}}$. Finally, $\|\cdot\|$ stands for the Euclidean norm of vectors from $\mathbb{R}^2$.

Now we introduce the following function sets:

$$\mathbb{V} = \{\mathbf{v} = (\mathbf{v}^1, \mathbf{v}^2) \in (H^1(\Omega^1))^3 \times (H^1(\Omega^2))^3 |\ \mathbf{v} = \mathbf{0} \text{ on } \Gamma_u\},$$

$$\mathbb{K} = \{\mathbf{v} \in \mathbb{V} |\ v_\nu \leq 0 \text{ on } \Gamma_c\},$$

$$X_\nu = \{\varphi \in L^2(\Gamma_c) |\ \exists \mathbf{v} \in \mathbb{V} :\ \varphi = v_\nu \text{ on } \Gamma_c\},$$

$$X_\nu' = \text{ dual of } X_\nu,$$

$$X_\nu^+ = \{\varphi \in X_\nu |\ \varphi \geq 0 \text{ on } \Gamma_c\}.$$

The cone of all non-negative elements of X_ν' will be denoted by $X_{\nu+}'$ and $\langle\cdot,\cdot\rangle$ is a duality pairing on $X_\nu' \times X_\nu$. Next we shall suppose that $\|\boldsymbol{\mathcal{F}}\mathbf{v}_t\|$ belongs to $X_{\nu+}$ for any $\mathbf{v} \in \mathbb{V}$.

We start with the following auxiliary problem: given $g \in X_{\nu+}'$, find $\mathbf{u} := \mathbf{u}(g) \in \mathbb{K}$ satisfying

$$a(\mathbf{u}, \mathbf{v} - \mathbf{u}) + \langle g, \|\boldsymbol{\mathcal{F}}\mathbf{v}_t\| - \|\boldsymbol{\mathcal{F}}\mathbf{u}_t\|\rangle \geq L(\mathbf{v} - \mathbf{u}) \quad \forall \mathbf{v} \in \mathbb{K}, \tag{3.1}$$

where

$$a(\mathbf{u},\mathbf{v}) = \int_\Omega \boldsymbol{\sigma}(\mathbf{u}) : \boldsymbol{\epsilon}(\mathbf{v})\, d\mathbf{x} := \int_\Omega \sigma_{ij}(\mathbf{u})\epsilon_{ij}(\mathbf{v})\, d\mathbf{x},$$

$$L(\mathbf{v}) = \int_\Omega \mathbf{f}^\top \mathbf{v}\, d\mathbf{x} + \int_{\Gamma_p} \mathbf{p}^\top \mathbf{v}\, ds, \quad \mathbf{u},\mathbf{v} \in \mathbb{V}.$$

It is easy to show that (3.1) has a unique solution for any $g \in X'_{\nu+}$. In addition, (3.1) is equivalent to the following minimization problem:

$$\left.\begin{array}{l} \text{Find } \mathbf{u} \in \mathbb{K} \text{ such that} \\ J_g(\mathbf{u}) \le J_g(\mathbf{v}) \quad \forall \mathbf{v} \in \mathbb{K}, \end{array}\right\} \qquad (\mathcal{P}(g))$$

where $J_g(\mathbf{v}) = \frac{1}{2}a(\mathbf{v},\mathbf{v}) - L(\mathbf{v}) + \langle g, \|\mathcal{F}\mathbf{v}_t\|\rangle$. Problem $(\mathcal{P}(g))$ is the variational formulation of contact problems with orthotropic friction and a *given* slip bound g. Let us suppose that $-\sigma_\nu(\mathbf{u}(g)) \in X'_{\nu+}$ for every $g \in X'_{\nu+}$. Then one can define the mapping $\Psi : X'_{\nu+} \mapsto X'_{\nu+}$ by

$$\Psi : g \mapsto -\sigma_\nu(\mathbf{u}(g)) \quad \forall g \in X'_{\nu+}.$$

Definition 3.1. By a weak solution of 3D contact problems with orthotropic Coulomb friction we mean any $\mathbf{u} \in \mathbb{K}$ such that $\Psi(-\sigma_\nu(\mathbf{u})) = -\sigma_\nu(\mathbf{u})$, i.e., $-\sigma_\nu(\mathbf{u})$ is a fixed point of Ψ in $X'_{\nu+}$.

Remark 3.2. In the weak formulation of this problem, the following unilateral and friction conditions are hidden:

(unilateral conditions)

$$u_\nu \le 0,\ \sigma_\nu(\mathbf{u}) \le 0,\ u_\nu\sigma_\nu(\mathbf{u}) = 0 \quad \text{on } \Gamma_c,$$

(friction conditions)

$$\mathbf{u}_t(\mathbf{x}) = \mathbf{0} \Longrightarrow \|\mathcal{F}^{-1}\boldsymbol{\sigma}_t(\mathbf{u}(\mathbf{x}))\| \le -\sigma_\nu(\mathbf{u}(\mathbf{x})),$$

$$\mathbf{u}_t(\mathbf{x}) \ne \mathbf{0} \Longrightarrow \mathcal{F}^{-1}\boldsymbol{\sigma}_t(\mathbf{u}(\mathbf{x})) = \sigma_\nu(\mathbf{u}(\mathbf{x}))\frac{\mathcal{F}\mathbf{u}_t(\mathbf{x})}{\|\mathcal{F}\mathbf{u}_t(\mathbf{x})\|}, \quad \mathbf{x} \in \Gamma_c.$$

We use the method of *successive approximation* for finding fixed points of Ψ in $X'_{\nu+}$:

$$\left.\begin{array}{l} \text{given } g^{(0)} \in X'_{\nu+}; \\ \text{set } g^{(k+1)} = \Psi(g^{(k)}),\ k = 0, 1, \ldots. \end{array}\right\} \qquad (3.2)$$

To get the new iteration $g^{(k+1)}$ one has to solve problem $(\mathcal{P}(g^{(k)}))$.

Remark 3.3. Let us note that convergence of (3.2) in continuous setting of our problem is not guaranteed. The situation is somewhat different in the discrete case (for details see [9, 11]).

Since $(\mathcal{P}(g))$, $g \in X'_{v+}$ is the heart of (3.2), we focus in the subsequent part on its efficient numerical solution. For a discretization of $(\mathcal{P}(g))$ we use a finite element method. First we choose a finite dimensional space $\mathbb{V}_h \subset \mathbb{V}$, $\dim \mathbb{V}_h = n(h)$ of piecewise polynomial functions of the Lagrange type over partitions $\mathcal{T}_h^k$ of $\overline{\Omega}^k$, which are compatible with the decomposition of $\partial\Omega^k$ into Γ_u^k, Γ_p^k, and Γ_c, $k = 1, 2$. These partitions will be constructed in such a way that $\mathcal{T}^1_{h|\Gamma_c} = \mathcal{T}^2_{h|\Gamma_c}$. In particular this means that if $\mathbf{v}_h = (\mathbf{v}_h^1, \mathbf{v}_h^2) \in \mathbb{V}_h$, where $\mathbf{v}_h^k := \mathbf{v}_{h|\Omega^k}$, then the degrees of freedom (function values in our case) of $\mathbf{v}_h^1$ and $\mathbf{v}_h^2$ on $\overline{\Gamma}_c$ are prescribed at the same nodes of $\mathcal{T}_h^k$ on $\overline{\Gamma}_c$. Typically, $\mathbb{V}_h$ is made of P_1 tetrahedral elements. Finally set $\mathcal{T}_h = \mathcal{T}_h^1 \cup \mathcal{T}_h^2$ which is the partition of the whole $\overline{\Omega}$. By $\mathcal{C}$ we denote the set of all nodes $\mathbf{a}_1, \ldots, \mathbf{a}_m$ of $\mathcal{T}_h$ which are located on $\overline{\Gamma}_c$. To simplify our presentation we shall suppose that $\overline{\Gamma}_u^k \cap \overline{\Gamma}_c = \emptyset$, $k = 1, 2$ and Γ_c is a flat part of $\partial\Omega$. Then the discretization of $\mathbb{K}$ is defined by

$$\mathbb{K}_h = \{\mathbf{v}_h \in \mathbb{V}_h |\ v_{h\nu}(\mathbf{a}_i) \le 0 \quad \forall i = 1, \ldots, m\},$$

where $v_{h\nu}(\mathbf{a}_i) := (\mathbf{v}_h^1(\mathbf{a}_i) - \mathbf{v}_h^2(\mathbf{a}_i))^\top \boldsymbol{\nu}$, $i = 1, \ldots, m$, i.e., the non-penetration conditions in $\mathbb{K}_h$ are prescribed at the nodes of $\mathcal{C}$ only using the fact that $\boldsymbol{\nu}$ is constant along Γ_c. The approximation of $(\mathcal{P}(g))$ reads as follows:

$$\left.\begin{aligned} &\text{Find } \mathbf{u}_h := \mathbf{u}_h(g) \in \mathbb{K}_h \text{ such that} \\ &J_g(\mathbf{u}_h) \le J_g(\mathbf{v}_h) \quad \forall \mathbf{v}_h \in \mathbb{K}_h. \end{aligned}\right\} \qquad (\mathcal{P}(g))_h$$

Next we rewrite $(\mathcal{P}(g))_h$ into the algebraic form, i.e. the problem expressed by means of the nodal displacement vectors $\bar{\mathbf{v}} \in \mathbb{R}^n$ of $\mathbf{v}_h \in \mathbb{V}_h$, where $n := n(h) = \dim \mathbb{V}_h$. Since first two terms of J_g define the quadratic, coercive functional, its algebraic form leads to a quadratic function with a positive definite, symmetric, block diagonal matrix $\mathbf{K}$. The frictional term will be evaluated using an appropriate cubature formula. Suppose that the slip bound g is represented by a continuous function. Then

$$\langle g, \|\boldsymbol{\mathcal{F}} \mathbf{v}_{ht}\| \rangle = \int_{\Gamma_c} g \|\boldsymbol{\mathcal{F}} \mathbf{v}_{ht}\|\, ds \approx \sum_{r=1}^{m} \omega_r\, g(\mathbf{a}_r) \|\boldsymbol{\mathcal{F}}(\mathbf{a}_r) \mathbf{v}_{ht}(\mathbf{a}_r)\|, \qquad (3.3)$$

where $\omega_r \in \mathbb{R}^1$, $r = 1, \ldots, m$ are weights of the used cubature formula. To express (3.3) and the whole problem $(\mathcal{P}(g))_h$ in the algebraic form, the following notation will be used: by $\mathbf{N}$ we denote an $(m \times n)$ matrix representing the linear mapping $\mathbf{v}_h \mapsto (v_{h\nu}(\mathbf{a}_1), \ldots, v_{h\nu}(\mathbf{a}_m)) \in \mathbb{R}^m$, $\mathbf{v}_h \in \mathbb{V}_h$. Similarly, $\mathbf{T}_j$, $j = 1, 2$ are $(m \times n)$ matrices of the linear mappings $\mathbf{v}_h \mapsto (v_{ht_j}(\mathbf{a}_1), \ldots, v_{ht_j}(\mathbf{a}_m)) \in \mathbb{R}^m$,

$\mathbf{v}_h \in \mathbb{V}_h$, where $v_{ht_j}(\mathbf{a}_r) := (\mathbf{v}_h^1(\mathbf{a}_r) - \mathbf{v}_h^2(\mathbf{a}_r))^\top \mathbf{t}_j$. Let $\mathbf{T}_{jr}$ be the r-th row of $\mathbf{T}_j$. Then $\bar{\mathbf{v}}_t^r := (\mathbf{T}_{1r}\bar{\mathbf{v}}, \mathbf{T}_{2r}\bar{\mathbf{v}})^\top \in \mathbb{R}^2$ is the vector of the tangential displacements at the node $\mathbf{a}_r$. Finally set $\boldsymbol{\mathcal{F}}_r := \boldsymbol{\mathcal{F}}(\mathbf{a}_r)$, $g_r := g(\mathbf{a}_r)$, and $\bar{\mathbf{g}} = (g_1, \dots, g_m)^\top$. Using this notation, $(\mathcal{P}(g))_h$ can be written as follows:

$$\left.\begin{aligned} &\text{Find } \bar{\mathbf{u}} \in \mathcal{K} \text{ such that} \\ &\mathcal{J}_{\bar{\mathbf{g}}}(\bar{\mathbf{u}}) \le \mathcal{J}_{\bar{\mathbf{g}}}(\bar{\mathbf{v}}) \quad \forall \bar{\mathbf{v}} \in \mathcal{K}, \end{aligned}\right\} \tag{$\mathcal{P}(\bar{\mathbf{g}})$}$$

where

$$\mathcal{J}_{\bar{\mathbf{g}}}(\bar{\mathbf{v}}) = \frac{1}{2}\bar{\mathbf{v}}^\top \mathbf{K}\bar{\mathbf{v}} - \bar{\mathbf{v}}^\top \bar{\mathbf{f}} + \sum_{r=1}^{m} \omega_r g_r \|\boldsymbol{\mathcal{F}}_r \bar{\mathbf{v}}_t^r\|$$

and

$$\mathcal{K} = \{\bar{\mathbf{v}} \in \mathbb{R}^n \,|\, \mathbf{N}\bar{\mathbf{v}} \le \mathbf{0}\}.$$

To release the constraints in $\mathcal{K}$ and to regularize the non-differentiable frictional term we use the duality approach. Let

$$\mathbf{X}(\bar{\mathbf{g}}) = \mathbb{R}^m_+ \times \mathbf{X}_t(\bar{\mathbf{g}})$$

be the set of the Lagrange multipliers, where

$$\mathbf{X}_t(\bar{\mathbf{g}}) = \{(\bar{\boldsymbol{\mu}}_{t_1}, \bar{\boldsymbol{\mu}}_{t_2}) \in \mathbb{R}^m \times \mathbb{R}^m \,|\, \|\boldsymbol{\mathcal{F}}_r^{-1} \bar{\boldsymbol{\mu}}_t^r\| \le \omega_r g_r,\ r = 1, \dots, m\}$$

and $\bar{\boldsymbol{\mu}}_t^r = (\mu_{t_1 r}, \mu_{t_2 r})^\top \in \mathbb{R}^2$ is the vector made of the r-th components of $\bar{\boldsymbol{\mu}}_{t_1}$ and $\bar{\boldsymbol{\mu}}_{t_2}$. It is easy to verify that

$$\sum_{r=1}^{m} \omega_r g_r \|\boldsymbol{\mathcal{F}}_r \bar{\mathbf{v}}_t^r)\| = \max_{(\bar{\boldsymbol{\mu}}_{t_1}, \bar{\boldsymbol{\mu}}_{t_2}) \in \mathbf{X}_t(\bar{\mathbf{g}})} \sum_{r=1}^{m} (\bar{\boldsymbol{\mu}}_t^r)^\top \bar{\mathbf{v}}_t^r.$$

Thus

$$\min_{\bar{\mathbf{v}} \in \mathcal{K}} \mathcal{J}_{\bar{\mathbf{g}}}(\bar{\mathbf{v}}) = \min_{\bar{\mathbf{v}} \in \mathbb{R}^n} \sup_{\bar{\boldsymbol{\mu}} \in \mathbf{X}(\bar{\mathbf{g}})} \mathcal{L}(\bar{\mathbf{v}}, \bar{\boldsymbol{\mu}}),$$

where $\mathcal{L}(\bar{\mathbf{v}}, \bar{\boldsymbol{\mu}}) = \frac{1}{2}\bar{\mathbf{v}}^\top \mathbf{K}\bar{\mathbf{v}} - \bar{\mathbf{v}}^\top \bar{\mathbf{f}} + \bar{\boldsymbol{\mu}}^\top \mathbf{B}\bar{\mathbf{v}}$ is the Lagrangian, $\bar{\boldsymbol{\mu}} = (\bar{\boldsymbol{\mu}}_\nu^\top, \bar{\boldsymbol{\mu}}_{t_1}^\top, \bar{\boldsymbol{\mu}}_{t_2}^\top)^\top \in \mathbf{X}(\bar{\mathbf{g}})$, and $\mathbf{B} = (\mathbf{N}^\top, \mathbf{T}_1^\top, \mathbf{T}_2^\top)^\top$ is the $(3m \times n)$ matrix. Instead of $(\mathcal{P}(\bar{\mathbf{g}}))$ we shall use its *saddle-point formulation*:

$$\left.\begin{aligned} &\text{Find } (\bar{\mathbf{u}}, \bar{\boldsymbol{\lambda}}) \in \mathbb{R}^n \times \mathbf{X}(\bar{\mathbf{g}}) \text{ such that} \\ &\mathcal{L}(\bar{\mathbf{u}}, \bar{\boldsymbol{\mu}}) \le \mathcal{L}(\bar{\mathbf{u}}, \bar{\boldsymbol{\lambda}}) \le \mathcal{L}(\bar{\mathbf{v}}, \bar{\boldsymbol{\lambda}}) \quad \forall (\bar{\mathbf{v}}, \bar{\boldsymbol{\mu}}) \in \mathbb{R}^n \times \mathbf{X}(\bar{\mathbf{g}}), \end{aligned}\right\}$$

or, equivalently,

$$\left.\begin{aligned} &\text{Find } (\bar{\mathbf{u}}, \bar{\boldsymbol{\lambda}}) \in \mathbb{R}^n \times \mathbf{X}(\bar{\mathbf{g}}) \text{ satisfying} \\ &\mathbf{K}\bar{\mathbf{u}} = \bar{\mathbf{f}} - \mathbf{B}^\top \bar{\boldsymbol{\lambda}}, \\ &(\bar{\boldsymbol{\mu}} - \bar{\boldsymbol{\lambda}})^\top \mathbf{B}\bar{\mathbf{u}} \le 0 \quad \forall \bar{\boldsymbol{\mu}} \in \mathbf{X}(\bar{\mathbf{g}}). \end{aligned}\right\} \qquad (\mathcal{M}(\bar{\mathbf{g}}))$$

One can easily show that $(\mathcal{M}(\bar{\mathbf{g}}))$ has a unique solution. Moreover its first component $\bar{\mathbf{u}}$ solves $(\mathcal{P}(\bar{\mathbf{g}}))$. Now we eliminate $\bar{\mathbf{u}}$ from the first equation: $\bar{\mathbf{u}} = \mathbf{K}^{-1}(\bar{\mathbf{f}} - \mathbf{B}^\top \bar{\boldsymbol{\lambda}})$ and substitute it into the second inequality. The resulting problem in terms of the Lagrange multipliers is equivalent to the following minimization problem:

$$\left.\begin{aligned} &\text{Find } \bar{\boldsymbol{\lambda}} \in \mathbf{X}(\bar{\mathbf{g}}) \text{ such that} \\ &\mathcal{S}(\bar{\boldsymbol{\lambda}}) \le \mathcal{S}(\bar{\boldsymbol{\mu}}) \quad \forall \bar{\boldsymbol{\mu}} \in \mathbf{X}(\bar{\mathbf{g}}), \end{aligned}\right\} \qquad (\mathcal{D}(\bar{\mathbf{g}}))$$

where $\mathcal{S}$ is the quadratic function with the symmetric, positive definite matrix $\mathbf{B}\mathbf{K}^{-1}\mathbf{B}^\top$ and the linear term $\bar{\mathbf{h}} = \mathbf{B}\mathbf{K}^{-1}\bar{\mathbf{f}}$. Notice that $(\mathcal{D}(\bar{\mathbf{g}}))$ has already the structure required by the algorithm KPRGP: the separated lower bounds for the components of $\bar{\boldsymbol{\lambda}}_\nu$ and the ellipsoidal constraints for the components of $(\bar{\boldsymbol{\lambda}}_{t_1}, \bar{\boldsymbol{\lambda}}_{t_2})$ as it follows from the definition of $\mathbf{X}(\bar{\mathbf{g}})$. Having $\bar{\boldsymbol{\lambda}}$ at our disposal we easily obtain $\bar{\mathbf{u}}$.

Remark 3.4. Model examples are solved by MatSol library [12] which uses the TFETI domain decomposition approach: each Ω^k, $k = 1, 2$ is divided into a finite number of subdomains involving "floating" blocks. To ensure continuity across subdomain interfaces and to satisfy the Dirichlet boundary conditions at the nodes of $\mathcal{T}_h$ on $\overline{\Gamma}_u$, the additional Lagrange multipliers are introduced. Then the resulting dual problem is given by the minimization of the quadratic function as in $(\mathcal{D}(\bar{\mathbf{g}}))$ but the set $\mathbf{X}(\bar{\mathbf{g}})$ contains, in addition, linear equality constraints. This fact requires an extension of the KPRGP algorithm called the SMALSE-M algorithm (for details see [7]). For realization of the problem with orthotropic Coulomb friction, we use an inexact implementation of the method of successive approximations (3.2) which performs only one iteration of the SMALSE-M in each step. In other words, the SAMLSE-M iterations and the successive approximations are performed by one outer loop.

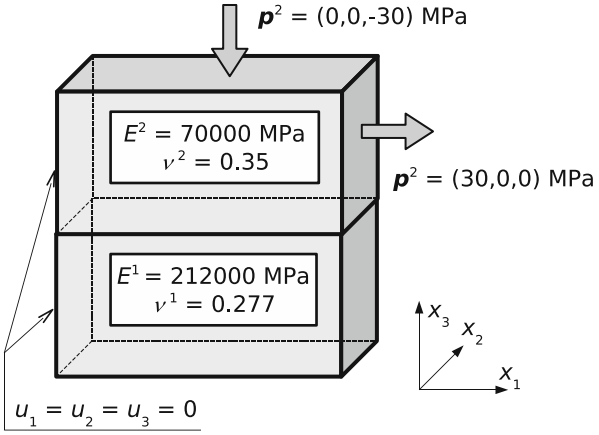

Fig. 1 Geometry of the problem

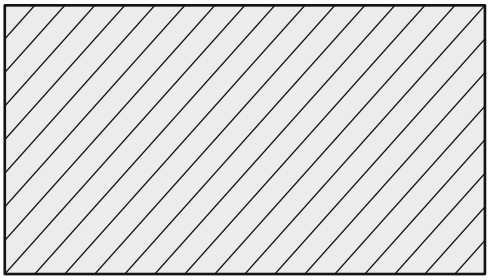

Fig. 2 Milled contact surface

4 Numerical Examples

Let us consider a 3D contact problem of two cantilever beams of sizes $2\times1\times1$ [m] in mutual contact with different coefficients of friction in two orthogonal directions to describe specially milled contact surface. The geometry, the prescribed boundary conditions, and material properties are specified in Fig. 1. The milled surface is depicted in Fig. 2. Finally, the volume forces are neglected and the coefficients of friction $\mathcal{F}_1$ and $\mathcal{F}_2$ on the contact interface are chosen in four different ways:

(a) Frictionless case: friction is neglected (Example 1);
(b) Isotropic case: $\mathcal{F}_1 = \mathcal{F}_2 = 0.3$ (Example 2);
(c) Orthotropic case: $\mathcal{F}_1 = 0.5$ in the direction $\mathbf{t}_1 = (1,0,0)^\top$ and $\mathcal{F}_2 = 0.1$ in $\mathbf{t}_2 = (0,1,0)^\top$ (Example 3);
(d) Orthotropic case: $\mathcal{F}_1 = 0.5$ in the direction $\mathbf{t}_1 = (\sqrt{2}/2, -\sqrt{2}/2, 0)^\top$ and $\mathcal{F}_2 = 0.1$ in $\mathbf{t}_2 = (\sqrt{2}/2, \sqrt{2}/2, 0)^\top$ (Example 4).

Case (d) corresponds to the real measurements, case (c) to incorrectly chosen tangential directions, case (b) to averaged coefficients which is a routinely used approach in engineering practise, and case (a) is for comparison purposes.

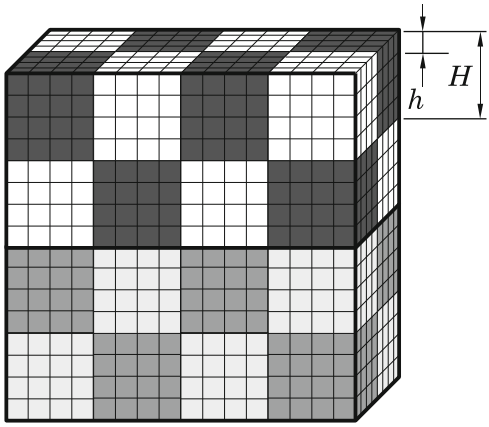

Fig. 3 Domain decomposition and the discretization

Each beam is divided into the same number of cubic subdomains with the decomposition step H and each subdomain is then decomposed into hexahedrons with the discretization step h; see Fig. 3. To demonstrate the behavior of our algorithms, we resolved the problem with varying discretizations and decompositions keeping $H/h = 10$.

The optimal choice of the parameters in the KPRGP is based on the analysis in [14] and on numerical experiments: we use $\Gamma = 1$, $\alpha \approx 2\|\mathbf{A}\|^{-1}$, adaptive values of ε depends on the precision achieved in the outer loop, and $\bar{\mathbf{x}}^{(0)}$ is determined by results from the previous outer iteration. The parameters of the SMALSE-M are chosen in agreement with [7]. The final relative stopping tolerance terminating the outer loop is 10^{-4} and the initial slip bound value in the discrete version of (3.2) is $\bar{\mathbf{g}}^{(0)} := \mathbf{0}$. The examples were computed by MatSol library [12] developed in Matlab environment and parallelized by Matlab Distributed Computing Server. For all computations we used 24CPUs of the HP Blade system, model BLc7000.

Example 1. We start with the frictionless case. The solution characteristics are summarized on the top of Table 1. We observe that the number of matrix–vector multiplications increases only moderately in agreement with the theory of [7]. The distribution of the normal contact stress Example 1 along the contact interface is depicted in Fig. 4.

Example 2. Let us consider the isotropic case *(b)*. This choice corresponds to the averaged friction coefficients of the real measurements for the surface from Fig. 2. The solution characteristics are summarized in the next part of Table 1. One can see that the number of outer iterations increases modestly with the size of the problem and the solution is more expensive compared with the previous example as follows from a higher number of the Hessian multiplications. The distribution of the normal contact stress along the contact interface is depicted in Fig. 5. In Figs. 6 and 7, we show the distributions of the Euclidean norm of the tangential contact stress and of displacements. The behavior of the contact stress inside the contact zone is seen in

Table 1 Solution characteristics for all examples

Number of subdomains	4	32	108	256
Primal variables	15,972	127,776	431,244	1,022,208
Dual variables	2,145	24,519	90,957	225,291
Equality constraints	24	192	648	1,536
Frictionless problem (Example 1)				
Bound constraints (active)	231 (11)	861 (15)	1,891 (20)	3,321 (35)
Outer iterations	11	11	9	9
Hessian multiplications	87	147	211	210
Isotropic case (Example 2)				
Bound constraints (active)	231 (11)	861 (64)	1,891 (135)	3,321 (246)
Circular constraints (active)	231 (220)	861 (830)	1,891 (1,847)	3,321 (3,270)
Outer iterations	11	15	19	22
Hessian multiplications	121	222	415	721
Orthotropic case, circular constraints (Example 3)				
Bound constraints (active)	231 (11)	861 (63)	1,891 (155)	3,321 (281)
Circular constraints (active)	231 (211)	861 (796)	1,891 (1,771)	3,321 (3,141)
Outer iterations	11	11	14	15
Hessian multiplications	149	262	487	665
Orthotropic case, ellipsoidal constraints (Example 3)				
Bound constraints (active)	231 (11)	861 (63)	1,891 (156)	3,321 (284)
Ellipsoidal constraints (active)	231 (213)	861 (798)	1,891 (1,784)	3,321 (3,151)
Outer iterations	11	10	16	17
Hessian multiplications	121	221	363	469
Orthotropic case, circular constraints (Example 4)				
Bound constraints (active)	231 (13)	861 (47)	1,891 (113)	3,321 (203)
Circular constraints (active)	231 (229)	861 (847)	1,891 (1,869)	3,321 (3,301)
Outer iterations	10	12	11	12
Hessian multiplications	126	315	332	344
Orthotropic case, ellipsoidal constraints (Example 4)				
Bound constraints (active)	231 (8)	861 (41)	1,891 (102)	3,321 (188)
Ellipsoidal constraints (active)	231 (220)	861 (846)	1,891 (1,860)	3,321 (3,301)
Outer iterations	15	24	28	29
Hessian multiplications	208	376	617	738

Fig. 8. The radiuses of small circles are given by the slip bound values $\mathcal{F}_1\lambda_{\nu,i}$, where $\mathcal{F}_1 = \mathcal{F}_2 = 0.3$ and $\lambda_{\nu i}$ is the component of $\bar{\boldsymbol{\lambda}}_\nu$ at the i-th contact node. The arrows in the circles represent the tangential contact stress.

Example 3. In this example we consider the orthotropic case *(c)* with the coefficients of friction $\mathcal{F}_1 = 0.5$ and $\mathcal{F}_2 = 0.1$ in the incorrectly chosen tangential directions $\mathbf{t}_1 = (1, 0, 0)^\top$ and $\mathbf{t}_2 = (0, 1, 0)^\top$, respectively. The results in Table 1 show that the computations with the circular constraints are more expensive than

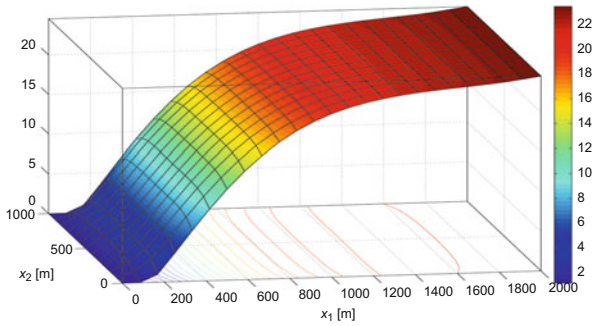

Fig. 4 Normal contact stress

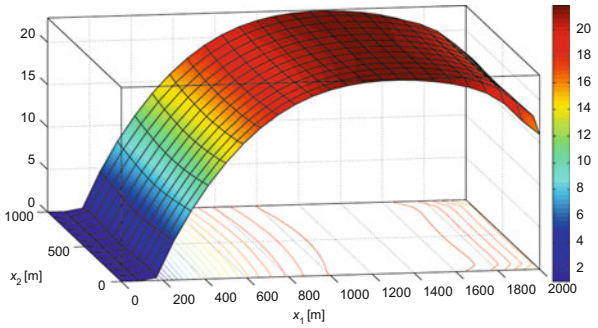

Fig. 5 Normal contact stress

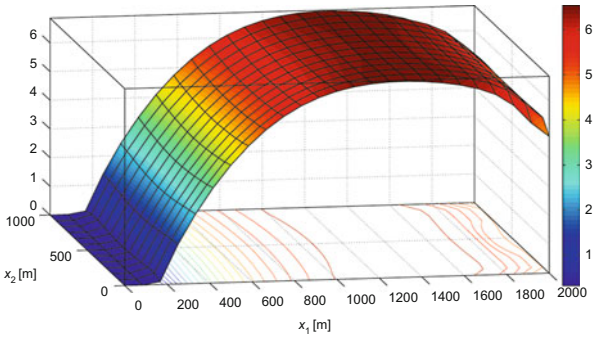

Fig. 6 The norm of the tangential contact stress

the ones with the original ellipsoidal constraints. This may be due to worse spectral properties of the Hessian matrix which increase the bound on the number of iterations; see Remark 2.1. In Figs. 9, 10, and 11, we depict the distributions of the normal contact stress and the standard and scaled Euclidean norms of the tangential

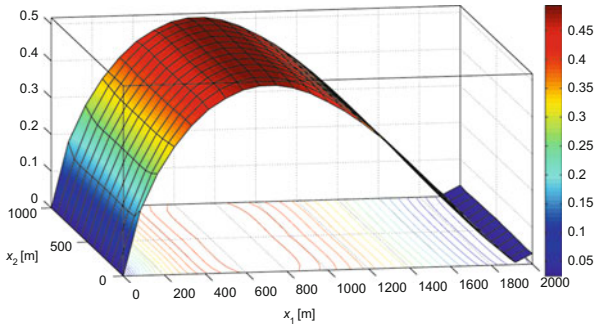

Fig. 7 The norm of the relative tangential contact displacements

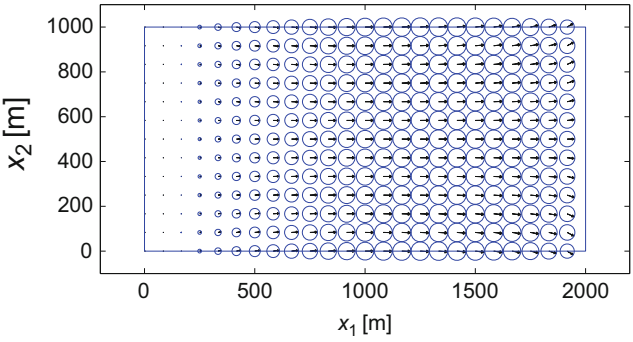

Fig. 8 Contact zone

contact stresses, respectively. The value of the scaled norm at the i-th contact node is defined as $\|\mathcal{F}_i^{-1}\bar{\boldsymbol{\lambda}}_t^i\|$, where $\bar{\boldsymbol{\lambda}}_t^i = (\lambda_{t_1 i}, \lambda_{t_2 i})^\top \in \mathbb{R}^2$ is the vector made of the i-th components of $\bar{\boldsymbol{\lambda}}_{t_1}$ and $\bar{\boldsymbol{\lambda}}_{t_2}$. The Euclidean norm of the relative tangential contact displacements is seen in Fig. 12. Finally, Figs. 13 and 14 show the behavior inside the contact zone. The semi-axes of ellipses are oriented by the directions $\mathbf{t}_1$ and $\mathbf{t}_2$ and their lengths are $\mathcal{F}_1\lambda_{vi}$ and $\mathcal{F}_2\lambda_{vi}$, respectively. Again, λ_{vi} are the components of $\bar{\boldsymbol{\lambda}}_v$ and the arrows in the ellipses represent the tangential contact stress.

Example 4. Finally, let us consider the orthotropic case *(d)* with the coefficients of friction $\mathcal{F}_1 = 0.5$ and $\mathcal{F}_2 = 0.1$ in the directions $\mathbf{t}_1 = (\sqrt{2}/2, -\sqrt{2}/2, 0)^\top$ and $\mathbf{t}_2 = (\sqrt{2}/2, \sqrt{2}/2, 0)^\top$, respectively. This setting corresponds to the milled surface depicted in Fig. 2. From Table 1 we can see that the circular constraints require less computations than the ellipsoidal ones. A heuristic argument explaining this fact is that the spectral properties of the new matrix after transformation of the ellipsoidal

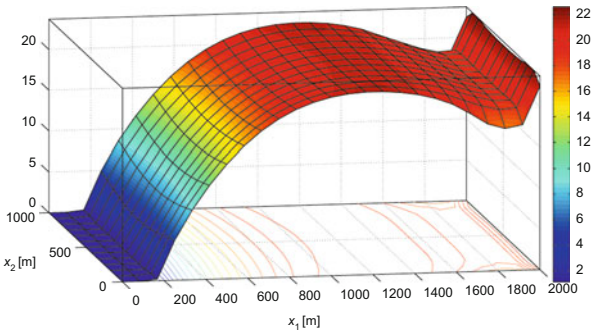

Fig. 9 Normal contact stress

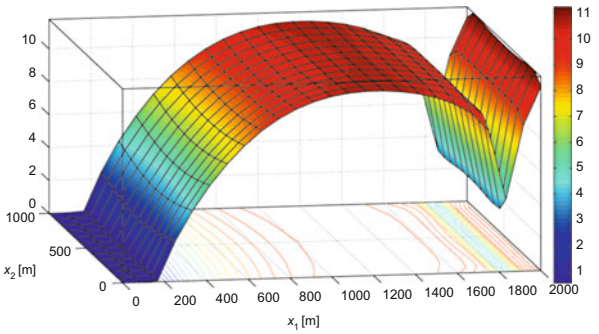

Fig. 10 The norm of the tangential contact stress

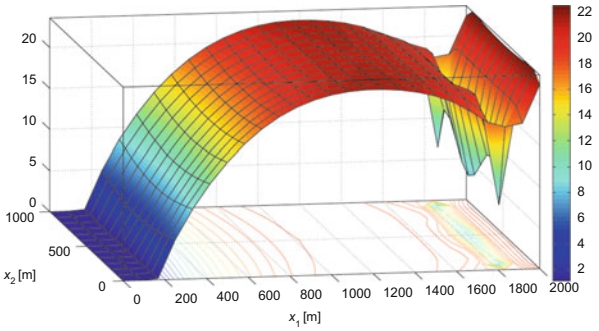

Fig. 11 The scaled norm of the tangential contact stress

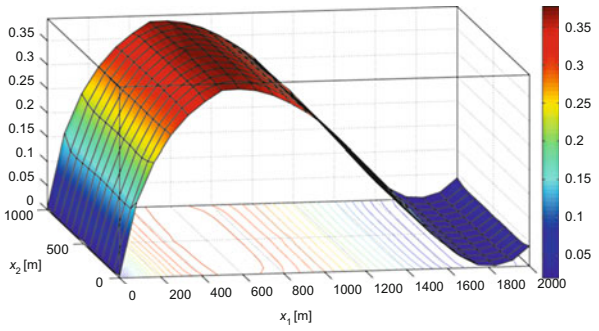

Fig. 12 The norm of the relative tangential contact displacements

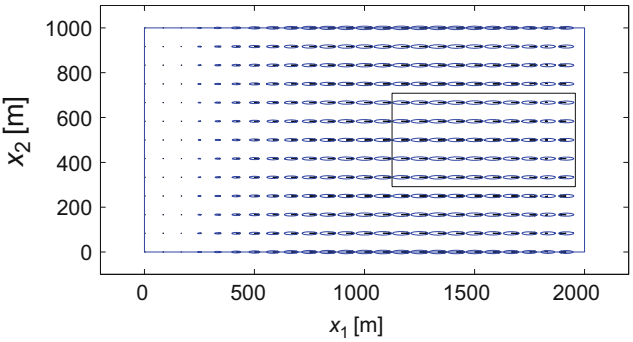

Fig. 13 Contact zone

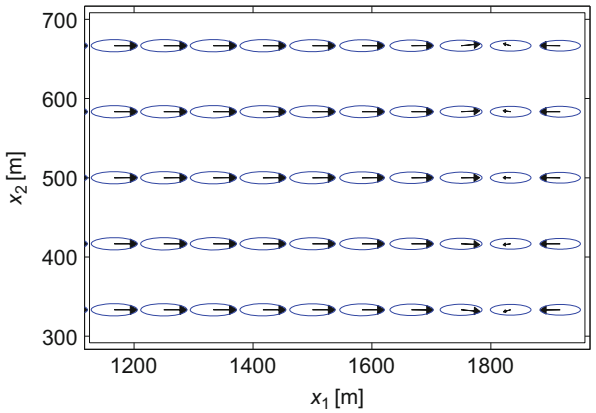

Fig. 14 Contact zone zoom

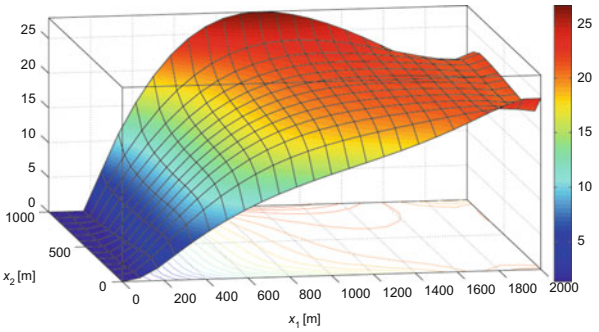

Fig. 15 Normal contact stress

constraints into the circular ones are sensitive to the orientation of the ellipses. In Figs. 15, 16, 17, 18, 19, and 20 we depict the same characteristics of the solution as in Example 3.

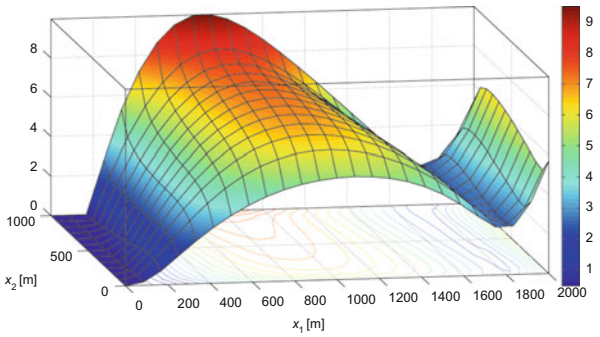

Fig. 16 The norm of the tangential contact stress

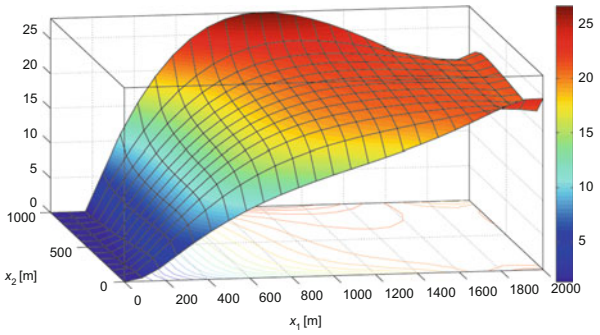

Fig. 17 The scaled norm of the tangential contact stress

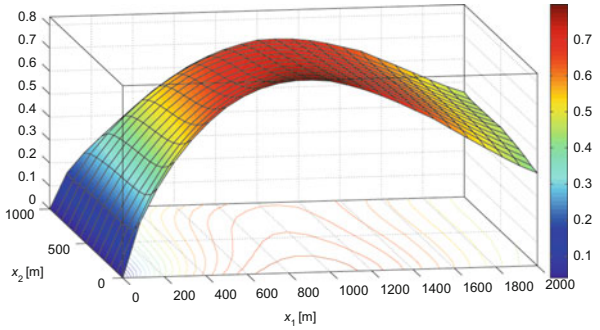

Fig. 18 The norm of the relative tangential contact displacements

Table 2 compares the computed displacements for different friction models. One can see the significant dependence of the results on the used friction model. Using the orthotropic friction law with correctly chosen tangential directions we get the results which are closer to the reality. An industrial application for the isotropic case may be found in [6].

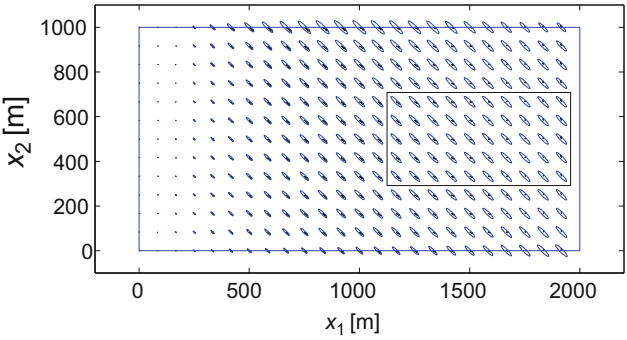

Fig. 19 Contact zone

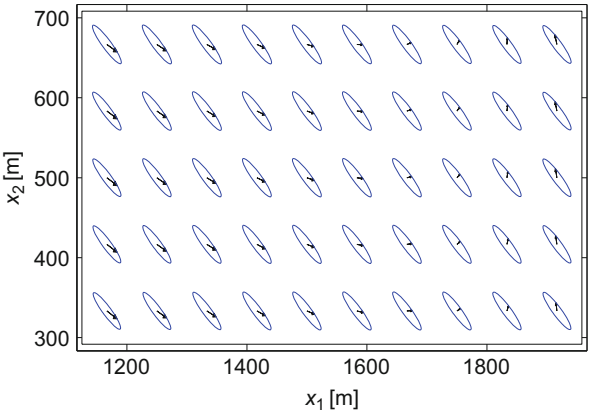

Fig. 20 Contact zone zoom

Table 2 Characteristic of the displacements for different friction models in the whole configuration

Friction model	$\max(\lvert u_1\rvert)$	$\max(\lvert u_2\rvert)$	$\max(\lvert u_3\rvert)$	$\max(\lVert \mathbf{u}\rVert)$
Case (*a*)	1.93765	0.13952	3.64374	4.12538
Case (*b*)	1.83178	0.12977	3.02874	3.53673
Case (*c*)	1.80919	0.12659	2.85510	3.37758
Case (*d*)	1.89417	0.30280	3.29204	3.80103

5 Conclusions

The paper deals with the KPRGP algorithm [14] for constrained minimization of strictly convex quadratic functions subject to simple bounds and separable ellipsoidal constraints. Since the algorithm uses the reduced gradient defined by the projection on the feasible set, the implementation requires to compute the

projections on ellipses. These projections are computed by a combination of the Newton and bisection methods.

Our study is motivated by the numerical solution of contact problems in linear elasticity with orthotropic Coulomb friction. The presented approach uses the method of successive approximations that requires to solve auxiliary contact problems with orthotropic Tresca friction in each iterative step. The algebraic dual formulation of the Tresca problem leads to the constrained minimization for which the KPRGP may be used. As an alternative to KPRGP one can use MPGP algorithm described in [5]. In order to increase the computational efficiency, we apply the finite element discretization based on the TFETI domain decomposition method. Since the TFETI introduces additional equality constraints in the algebraic problem, we apply the SMALSE-M algorithm [7] in which the KPRGP is included as the inner loop. The outer loop of the SMALSE-M is based on the augmented Lagrangian method. The important property of the SMALSE-M is the fact that the number of iterations needed to get a solution with a given accuracy is uniformly bounded (with respect to the size of the problem) provided that the spectrum of the Hessian is confined in a given interval (i.e., the algorithm is scalable). This assumption is satisfied, if the ratio between the maximal diameter of the subdomains H and the norm of the finite element partitions h is fixed and the Hessian is normalized in the spectral norm [6]. Let us recall that the scalability can be proven only for the frictionless case and Tresca friction but we observed it experimentally also for some examples with Coulomb fiction.

Acknowledgements The work was supported by the ESF OPTPDE Research Programme. The first author acknowledges also the support of the grant GAČR P201/12/0671. The second and the third author acknowledge the support of the European Regional Development Fund in the IT4 Innovations Centre of Excellence project (CZ.1.05/1.1. 00/02.0070).

References

[1] A. Ben-Tal, A. Nemirovski, *Lectures on Modern Convex Optimization* (SIAM, Philadelphia, 2001)
[2] S. Boyd, L. Vandenberghe, *Convex Optimization* (Cambridge University Press, Cambridge, 2004)
[3] A. Conn, N. Gould, P. Toint, *Trust Region Methods* (SIAM, Philadelphia, 2000)
[4] Z. Dostál, *Optimal Quadratic Programming Algorithms: With Applications to Variational Inequalities* (Springer, Berlin/Heidelberg/New York, 2009)
[5] Z. Dostál, T. Kozubek, An optimal algorithm and superrelaxation for minimization of a quadratic function subject to separable convex constraints with applications. Math. Programming **135**, 195–220 (2012)
[6] Z. Dostál, T. Kozubek, A. Markopoulos, T. Brzobohatý, V. Vondrák, P. Horyl, Theoretically supported scalable TFETI algorithm for the solution of multibody 3D contact problems with friction. Comput. Methods Appl. Mech. Eng. **205**, 110–120 (2012)
[7] Z. Dostál, R. Kučera, An optimal algorithm for minimization of quadratic functions with bounded spectrum subject to separable convex inequality and linear equaity constraints. SIAM J. Opt. **20**, 2913–2938, 2010.

[8] G.H. Golub, C. F. Van Loan, *Matrix Computation* (The Johns Hopkins University Press, Baltimore, 1996)
[9] J. Haslinger, Approximation of the Signorini problem with friction, obeying Coulomb law. Math. Meth. Appl. **5**, 422–437 (1983)
[10] J. Haslinger, I. Hlaváček, J. Nečas, Numerical methods for unilateral problems in solid mechanics, in *Handbook of Numerical Analysis*, vol. IV, ed. by P.G. Ciarlet, J.-L. Lions (North-Holland, Amsterdam, 1996), 313–485
[11] J. Haslinger, R. Kučera, T. Ligurský, Qualitative analysis of 3D elastostatic contact problems with orthotropic Coulomb friction and a solution dependent coefficients of friction. J. Comput. Appl. Math. **235**, 3464–3480 (2011)
[12] T. Kozubek, A. Markopoulos, T. Brzobohatý, R. Kučera, V. Vondrák, Z. Dostál, *MatSol - MATLAB Efficient Solvers for Problems in Engineering*. http://industry.it4i.cz/en/products/matsol
[13] R. Kučera, Minimizing quadratic functions with separable quadratic constraints. Optim. Meth. Soft. **22**, 453–467 (2007)
[14] R. Kučera, Convergence rate of an optimization algorithm for minimizing quadratic functions with separable convex constraints. SIAM J. Optim. **19**, 846–862 (2008)
[15] J. Nečas, I. Hlaváček, *Mathematical Theory of Elastic and Elasto-Plastic Bodies: An Introduction*. Studies in applied mechanics, vol. 3 (Elsevier Scientific Publishing Co., Amsterdam/New York, 1980)
[16] J.B. Rosen, The gradient projection method for nonlinear programming. Part II. Nonlinear constraints. J. Soc. Indust. Appl. Math. **9**, 515–532 (1961)
[17] S.J. Wright, *Primal-Dual Interior-Point Methods* (SIAM, Philadelphia, 1997)
[18] H.W. Zhang, A.H. Liao, Z.Q. Xie, B.S. Chen, H. Wang, Some advances in mathematical programming methods for numerical simulation of contact problems, in *Proceedings of the IUTAM Symposium on Computational Methods in Contact Mechanics*, ed. by P. Wriggers, U. Nackenhorst (Springer, Berlin/Heidelberg/New York, 2007), 33–56